Defense Technical Information Center
Compilation Part Notice

ADP013469

TITLE: Using Adaptive Estimation to Minimize the Number of Samples Needed to Develop a Radiation or Scattering Pattern to a Specified Uncertainty

DISTRIBUTION: Approved for public release, distribution unlimited

This paper is part of the following report:

TITLE: Applied Computational Electromagnetics Society Journal. Volume 17, Number 3

To order the complete compilation report, use: ADA412338

The component part is provided here to allow users access to individually authored sections of proceedings, annals, symposia, etc. However, the component should be considered within the context of the overall compilation report and not as a stand-alone technical report.

The following component part numbers comprise the compilation report:
ADP013469 thru ADP013476

USING ADAPTIVE ESTIMATION TO MINIMIZE THE NUMBER OF SAMPLES NEEDED TO DEVELOP A RADIATION OR SCATTERING PATTERN TO A SPECIFIED UNCERTAINTY

Edmund K. Miller, Los Alamos National Laboratory (retired)
3225 Calle Celestial
Santa Fe, NM 87506-1213
ekmiller@prodigy.net

ABSTRACT
Obtaining far-field patterns in electromagnetics or acoustics, although generally not as computationally expensive as solving for the sources induced on an object, can none-the-less at times be a substantial fraction of the overall computer time required for some problems. This can be especially the case in determining the monostatic radar cross section of large objects, since the current distribution must be computed for each incidence angle, or when computing the radiation patterns of large reflector antennas using physical optics. In addition, when employing the point sampling and linear interpolation of the far field that is most often used to develop such patterns, it can be necessary to sample very finely in angle to avoid missing fine details such as nulls. A procedure based on model-based parameter estimation is described here that offers the opportunity of reducing the number of samples needed while developing an easily computed and continuous representation of the pattern. It employs windowed, low-order, overlapping fitting models whose parameters are estimated from the sparsely sampled far-field values. The fitting models themselves employ either discrete-source approximations to the radiating currents or Fourier models of the far field. For the cases investigated, as few as 1.5 to 2 samples per far-field lobe are found to be sufficient to develop a radiation-pattern estimate that is accurate to 0.1 dB, and 2.5 samples per lobe for a simple scatterer. In general, however, the sampling density is not determined by the lobe count alone, but by the effective rank of the field over the observation window, which in turn is a function of both the aperture size and the spatial variation of the source distribution within that aperture.

1. INTRODUCTION
An important goal of all numerical modeling is that of minimizing the number of samples needed of the relevant observables and equations so as to minimize the total computer operation count (OC) (or the computer cost) while achieving a desired accuracy, or equivalently reducing the uncertainty to a specified level, in the computed results. This topic is considered below in the context of computing radiation and scattering patterns in electromagnetics. The goal of particular interest here concerns minimizing the number of far-field pattern samples that are required to represent a radiation pattern and/or the number of incidence angles that are required to develop a monostatic backscatter radar-cross section (RCS) pattern. An added benefit of the procedure described below is that of obtaining an estimate of the uncertainty in the pattern that is developed.

The approach taken employs model-based parameter estimation (MBPE) [1]. This is a procedure that uses reduced-order, physically based fitting models (FMs) whose parameters are computed from samples of first-principles generating models (GMs) such as Maxwell s Equations. Computation of a FM sample is trivial compared with one evaluated from a GM for large, complex problems, potentially requiring orders-of-magnitude less computing time. This makes it possible, using the FM, to develop an essentially continuous representation of physical observables of interest as opposed to the pointwise characterization that is usually accepted when the cost of each GM evaluation is large. A list of acronyms used in the article follows the references.

2. BACKGROUND
One of the most frequently encountered problems in electromagnetic field computations is that of determining a radiation or scattering pattern from a current distribution(s) known over some surface. For antenna applications, usually a single current distribution is of interest, while for RCS computations, a new current distribution arises for each incidence angle of a plane-wave exciting field. In either case, the far field is usually needed at enough points to develop a smooth, in effect continuous, approximation of the overall pattern in one or more planes. The required number of radiation-pattern samples and resulting OC are proportional to the maximum body dimension, L, in the plane in which the pattern is being computed. Furthermore, the number of current samples on the surface, S, is itself is proportional to the body s surface area, i.e., $S \propto L^2$. As L, and therefore S, increases, the far-field computation can become a significant cost in obtaining radiation and scattering patterns. Thus, reducing the number of angle samples could be worthwhile in terms of reducing the overall computer cost of obtaining the radiation pattern(s) of a large antenna or RCS of a large scatterer

Some previous work by the author [2,3] and others [4,5] has described an approach that uses MBPE to decrease the number of samples that are needed to determine a far-field pattern. The work presented in [2,3], is briefly summarized and extended here, especially with respect to how the errors in the pattern can be estimated and controlled and how the pattern itself is modeled. Further examples of efficient pattern computation can be found in the work of Bucci and his various collaborators who have developed signal-processing-like techniques for computing far-field patterns [see for example 6, 7, and 8].

3. CHOOSING THE QUANTITY TO MODEL
Estimating a far-field pattern using MBPE requires choosing the kind of reduced-order FM that is to be used and to what observable that FM is to be applied. Two obvious choices for minimizing the number of pattern samples or incidence angles are available: 1) to model the current distribution; or 2) to model the far-field pattern. Furthermore, there are two ways in which the current distribution itself might be modeled. These various choices are briefly summarized below.

3.1 Modeling a Current (or Aperture) Distribution
The two approaches to be discussed here for modeling the current (or aperture) can be best described as Discrete-Source Approximations (DSAs). The current over the surface of the object under consideration or field over an aperture is replaced by a

linear array of discrete, or point, sources aligned in space as is described below. (Other point-source geometries might also be used; attention is limited here to a linear geometry). The parameters of the DSA model are obtained by fitting it to far-field samples obtained from the usual integration of the actual current distribution. The DSA is then used to approximate the pattern between these samples to thereby obtain a continuous estimate of the pattern without requiring additional current integrations.

3.1.1 Using A Prony Model

Prony s method (or its equivalent) can be used for the DSA computation, using as a FM [9]

$$F(\theta) = \sum_{\alpha=1}^{P} S_{\alpha} e^{ikd_{\alpha}\cos(\theta)}$$

(1)

which involves P point sources of strengths S_{α} located at positions d_{α} along the axis of the DSA° array, with θ the angle to the far field measured from that axis. There being 2N unknown parameters in Eq. 1, the Prony DSA (PDSA) thus requires 2N far-field samples of the actual pattern. Furthermore, these 2N samples need to be spaced uniformly in $\cos(\theta)$, a feature that makes PDSA less suitable for the adaptive-sampling approach described next. A possible advantage, however, of finding the locations of the discrete sources is the possibility of developing an approximate image of the source whose far field is being sampled.

There are two different candidate DSA geometries that might be considered. In the first, shown in Fig. 1a, the DSA axis is fixed and a sequence of angle windows are rotated about this axis over the complete range of observation angles of interest. In the second, shown in Fig. 1b, the DSA axis is itself rotated to be perpendicular to the angle that defines the midpoint of each angle window used for the successive DSA computations. Note that L varies in proportion to the length of the object as seen from the center of the observation window when using the approach of Fig. 1b whereas L is fixed at the maximum linear dimension of the object in the observation plane for approach 1a.

3.1.2 Using A Specified DSA

The specified DSA (SDSA) model is the same as Eq. 1 except that, since the source locations are now specified, only the N source strengths S_{α} are unknowns. As for the Prony DSA, samples of the actual far-field are used to obtain the discrete-source strengths. In contrast to the Prony model, however, the pattern samples are not constrained in their placement but can be arbitrarily located in angle and only N are needed, two distinct over the Prony model. For the SDSA results presented here, the sources are equally spaced along the array axis, with the source numbers 1 and N located at the ends of the aperture L using the configuration shown in Fig. 1a. As the order, i.e., number of sources used in a particular SDSA FM, is increased, the source spacing is therefore systematically decreased in proportion to the number of sources that are used.

3.2 Modeling the Pattern

An alternative to using a DSA for the pattern estimation is to model the pattern itself, using a Fourier series, an approach

denoted as the Fourier Series Pattern Model (FSPM). In this case the FM can be developed as [2]

$$F(\theta) = \sum_{\alpha=S}^{F} R_{\alpha} e^{i\alpha\theta} + \sum_{\alpha=S'}^{F} R'_{-\alpha} e^{-i\alpha\theta}$$

(2)

where we set F equal to Int(L + 1), with Int(X) denoting the value of X rounded off to the nearest lower integer. Also, 2F - S - S = N with N the total number of terms in the FM, S † S † S + 1, and R_{α} and $R_{-\alpha}$ are the amplitudes of the positive and
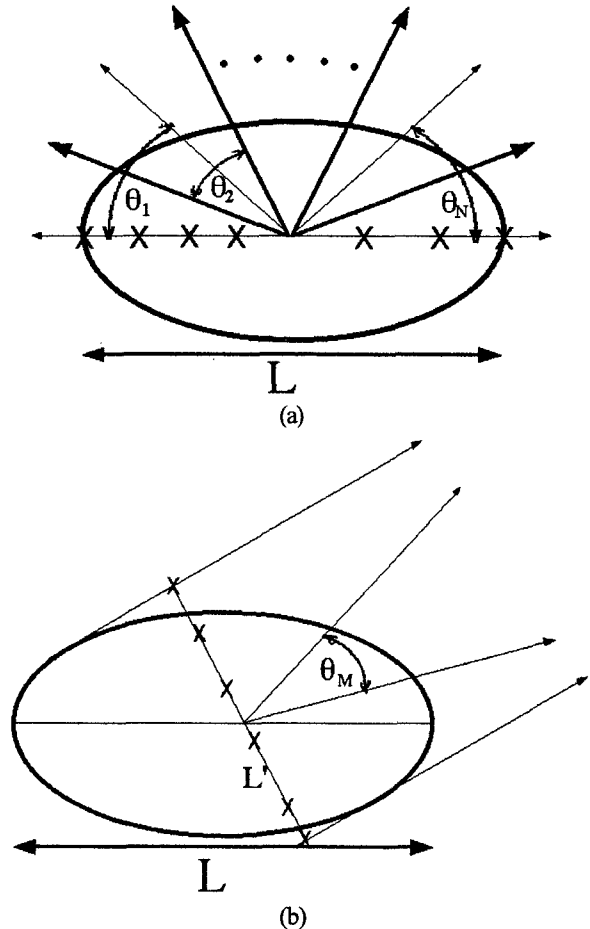

Figure 1. Two ways of implementing the Discrete-Source Array Fitting Model. In (a) the sampling window (denoted by alternately light and heavy lines) rotates in angle about the long axis of the object while the DSA FM axis remains fixed along which the discrete sources are located. In (b), on the other hand, the sampling aperture L' is rotated with respect to the long axis of the object and the sampling window is bisected by a line perpendicular to it. For the case of the PDSA, an N-source FM requires a minimum of 2N field samples. Both the source locations (indicated by the X's) and their strengths are determined by sampling the far field as a function of $\cos(\theta)$, where generally the sources will be non-uniformly spaced. Alternatively, for the SDSA used to obtain the results presented here, the configuration (a) was used with N sources uniformly spaced along the array axis, thus requiring only N field samples for computation of their strengths.

negative modes respectively. As for the specified DSA, N far-field samples are required to quantify the parameters of the FSPM. Note that the Fourier approach yields estimates of the far-field Fourier components directly, as contrasted with either of the DSA FMs where the source strengths, and locations as well for the PDSA, are the parameters being computed. Ultimately, however, the differences between the SDSA and the FSPM are rather slight, differing most in the former having an observation-angle dependence given by $\exp[ikd\cos(\theta)]$ while the latter depends on $\exp(i\alpha\theta)$.

3.3 Adaptive Estimation Using Windowed, Overlapping Fitting Models

To be effectively implemented, any adaptive numerical procedure requires an error estimate. For the specific problem of adaptive pattern estimation, the error estimate is used to determine whether a given FM is accurate enough, and if not, where in angle a new sample should be located. Various FM configurations might be considered in this application. For example, a single FM might be used to span the entire angle window of interest with an initial set of sample angles, S, chosen for GM evaluation. A subset of these GM samples, S-1, could be used to obtain the S-1 parameters of FM(S-1) while all S GM samples could be similarly used to find the S parameters of FM(S). These two FMs could then be sampled more finely, by a factor of 10 or so, in angle than was used for the initial GM sampling, with the difference between them serving as an error measure. If the error measure exceeds the allowable uncertainty specified by the modeler, the S+1 th GM sample would be added at the angle where the difference between FM(S-1) and FM(S) is greatest. The parameters of FM(S+1) could then be computed and the difference between FM(S) and FM(S+1) obtained. The process would be systematically continued until the maximum difference between FM(S+k-1) and FM(S+k) satisfies the uncertainty specification, with S+k the total number of GM samples required. The initial number of GM samples to be used, S, would be chosen to be proportional to the number of pattern lobes expected over the observation window.

Using a single FM to cover an entire pattern would generally not be the best approach, however, partly due to the growing cost of the FM computation itself, but more importantly due to the fact that the condition number of the data matrix needing solution for the FM parameters may increase unacceptably, especially for a large number of pattern lobes. Instead, as is done here, a number of windowed, lower-order (i.e., fewer parameters) overlapping FMs are used. Each FM shares two or more GM samples with its neighbors, as is illustrated conceptually in Fig. 2 where there are a total of N FMs. As above, after their parameters have been evaluated, the FMs are evaluated more finely in angle than was the GM pattern initially, and the differences between the sets of overlapping FMs are computed. A new GM sample then is added where the maximum difference between all sets of overlapping FMs is found to occur. The respective parameters of the affected FMs (i.e., those whose windows contain the new sample angle) are then updated, with the process of computing FM differences and new GM samples continuing until the specified uncertainty is satisfied over the entire pattern window.

An appropriate choice for the number of FMs for a given problem might require some experimentation. If it s desired to keep the order of all FMs below some specified value, then based on the computer experiments done in getting the results presented below, each FM should have an angle window that spans just a

few pattern lobes, say three or four at most. The number of lobes to be expected can generally be estimated from the size of the aperture whose pattern is being modeled. However, it may happen that adding a new GM sample to a FM causes its to rank exceed some specified limit. By dividing such a FM into two lower-order, overlapping ones, the problem of excess FM rank can be avoided and the initial number of FMs will not be so important.
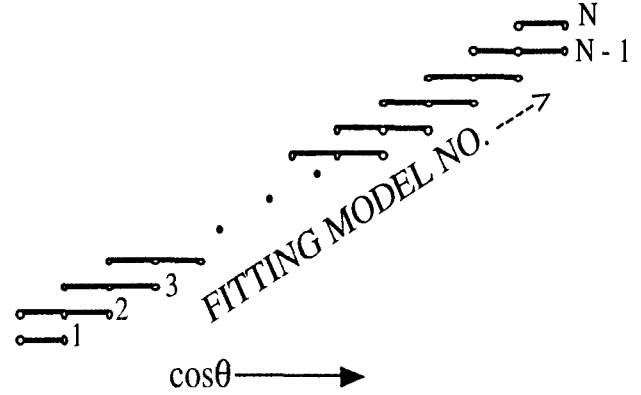

Figure 2. A conceptual illustration of the use of overlapping fitting models for adaptive sampling of a far-field pattern. The horizontal lines indicate the angular extent of each FM with the open circles showing where the pattern (or GM) is initially sampled. In this particular case, all interior FMs begin with three GM samples while those at either end use only two, for a total of N + 1 starting samples. Additional GM samples are systematically located where the maximum difference occurs between two overlapping FMs until a specified convergence criterion has been satisfied. Only two FMs overlap in any of the observation windows here, but other overlap arrangements could be used as well.

3.4 Specification of the Fitting-Model Error and Computing the Final Pattern Estimate

In contrast to specifying a fixed FM difference, or fitting-model error (FME), between overlapping FMs as was done in [2,3], the maximum FME can also be scaled relative to how the magnitudes of the far-field samples vary. For example, as the magnitude decreases the FME might be proportionately increased to accommodate the fact that side-lobe maxima may not be needed to the same accuracy as the main lobe. In the results to follow, the maximum permitted FME at the observation angle θ is given by

$$FME(\theta) = A_1 + A_2\left[\, |GM(\theta_{max}) - \frac{1}{M}\sum_{\alpha=1}^{M} FM_\alpha(\theta)| \,\right]$$

(3)

where A_1 and A_2 are specified parameters, $GM(\theta_{max})$ is the maximum value of the pattern being modeled, and $FM_\alpha(\theta)$ is the value of the a th FM at θ where a total of M FMs overlap. The parameter A_1 determines the maximum acceptable FME in the vicinity of the peak(s) of the GM. The parameter A_2 increases the allowable FME in proportion to the decrease in the FM values relative to $GM(\theta_{max})$. For the results that follow, the nominal values for A_1 and A_2 were 0.1 and 0.05 dB, respective-

ly, but FME(θ) limited to a maximum value of 3 dB. There are many possible variations that might be used for setting the acceptable error or uncertainty, among which would be relaxing the desired accuracy in certain angular regions or increasing it in others consistent with the requirements of a particular application.

The final pattern estimate is then obtained by computing the average of the successively overlapping FMs as the observation angle is scanned over the angle pattern. Thus, for M overlapping FMs at angle θ we would have

$$F_{ave,M}(\theta) = \frac{1}{M}[F_i(\theta) + F_{i+1}(\theta) + \cdots + F_{i+M-1}].$$

(4)

For the results presented below, M = 2 was used.

Note that in addition to controlling the adaptation process, the error specification provides a measure of the uncertainty in the average FM values of Eq. 4. Since Eq. 3 gives the maximum variation permitted between the FMs that overlap at a given angle, it s proposed that

$$F_{ave,M\pm}(\theta) = F_{ave,M}(\theta) \pm \frac{1}{2}FME(\theta)$$

(5)

will yield realistic upper and lower error-bound estimates for the average pattern values. That Eq. 5 does indeed provide a realistic error bound relative to the FM estimates of GM is demonstrated in the following examples.

It s worth emphasizing that, in contrast to using an entire-domain basis for the far field, cylindrical- or spherical-wave expansions, for example, the windowed approach employed here together with discrete point sources can be applied to smaller, or limited, angular sectors with no computational penalty. Also observe that in implementing the SDSA, angle sampling is done in terms of cos(θ) rather than θ. This is because the pattern lobes tend to be distributed uniformly in terms of the former variable.

To summarize then, the following steps are involved in the MBPE modeling of radiation and scattering patterns:

1) The quantity to be modeled, i.e., the source distribution or pattern itself, is first selected.

2) The total angle window over which the pattern is to be estimated is specified.

3) The number of pattern lobes, L, that are anticipated over the angle window of interest, considering the aperture size in wavelengths whose pattern is to be found, is estimated.

4) The number, N, of initial fitting models to be used then needs to be chosen. Choosing a value for N between L/2 and 2L/3, with L expressed in wavelengths, should provide a reasonable starting point, noting that the smaller the value of N that is used the larger will be the required FM order.

5) The configuration of the FM overlap then needs to be selected. This can be fairly flexible. Arranging each window to be half overlapped with its nearest neighbors seems to be a good choice. Note that using half-overlapped FMs leads naturally to a minimum of 3 initial GM samples per FM window as shown in Fig. 2.

6) Finally, the kind of FM error to be used and its numerical parameters, as in Eq. (3), must be specified.

4. USING THE SPECIFIED DISCRETE-SOURCE APPROXIMATION

In previous work [2,3] the FSPM approach was described and some initial results presented, demonstrating that the far-field pattern could be estimated to an amplitude uncertainty of 0.01 (about 0.05 dB) using only ~ 3 to 3.5 samples per lobe. Several results obtained using the alternate SDSA model are presented here together with an illustration of how the model performance depends on the uncertainty specification. The particular patterns used for testing the MBPE approach here were chosen as being representative of the kinds of patterns encountered in typical applications, as well as their having closed-form analytical expressions, except for the last example of the random-source array.

4.1 The Far Radiated Field of the Uniform Current Filament

The far field, $F(\theta)_{UCF}$, of a uniform current filament (or uniform aperture) is proportional to [10]

$$F(\theta)_{UCF} = L\frac{\sin[\pi L\sin(\theta)]}{\pi L\sin(\theta)}$$

(6)

where the filament length L is expressed in wavelengths and the observation angle θ is measured from the filament axis. A total of N = 13 FMs was used for an L = 20-wavelength UCF, arranged as shown in Fig. 2, with the parameters of Eq. 3 given by A_1 = 0.1 and A_2 = 0.05 dB. Thus, all FMs initially have three GM samples except for those on either end, which have only two. This results in each FM sharing two samples with its nearest neighbors except for those on the end, which overlap with one adjacent FM. Applying the SDSA to GM samples of Eq. 6 yields the results of Fig. 3, normalized to a maximum of 0 dB, where the upper and lower error-bound estimates for the pattern peaks, using Eq. 5, and the actual pattern from Eq. 6 are plotted. The actual pattern is seen to lie between the upper- and lower-bound peaks throughout the entire window. In Fig. 4 the average values of the overlapping FMs from Eq. 4, FM_{ave}, are compared with the actual pattern, where 34 of the 35 GM samples used for computing the final FM parameters are also shown. The maximum difference between the actual pattern and FM_{ave} is consistent with the error specification of Eq. 4 and the numerical values used for its parameters. With 35 samples needed to estimate a pattern having 20 lobes or maxima, 1.75 samples are required per lobe for the UCF.

The behavior of three different error measures for the L = 20 UCF is presented in Fig. 5 as a function of the number of GM samples used for computing the FM parameters. The upper plot on this graph shows the maximum difference between all pairs of the 13 finely sampled, overlapping FMs as a function of the number of GM samples used for their computation. The middle plot exhibits the difference between all pairs of overlapping FMs averaged over the angles they commonly sample. The bottom

plot displays the angle-averaged difference between FM_{ave} and the actual pattern, or the GM. Of these three, only the first two would be available in actual application since the GM samples needed to compute the last error measure would be limited to those available up to that point in the adaptation process. It s useful to include the latter error measure, however, as the difference between the FM_{ave} and the GM provides a reality check on the MBPE performance.

Observe that the difference between the overlapping FMs for this example always exceeds the corresponding FM_{ave} - GM difference. This shows that the FM-FM error measure provides a conservative, or high-side, estimate of the error (or uncertainty) in FM_{ave} relative to the true GM values. Note also that the maximum FM difference does not decline monotonically. This is because updating two FMs can at times increase the maximum differences that then results with their overlapping neighbors.
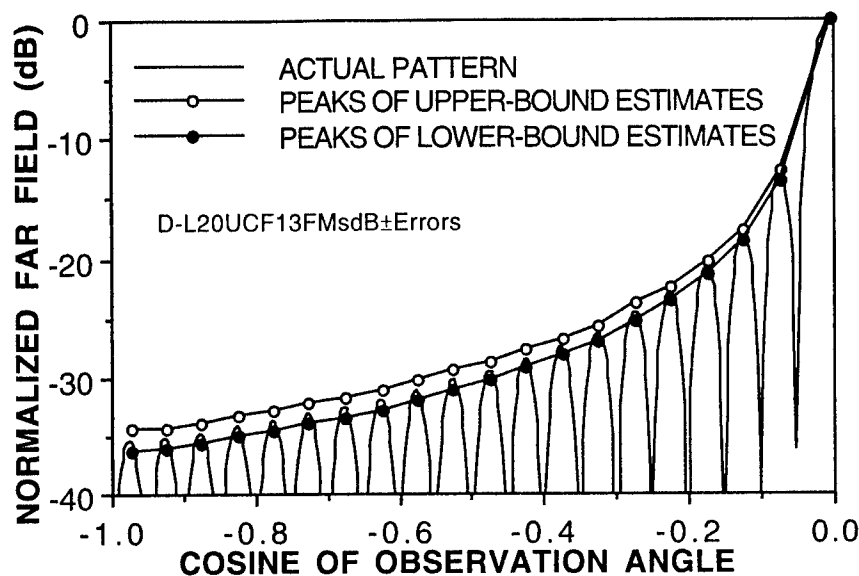

Figure 3. One quadrant of the normalized radiation pattern for the field of an L = 20 (wavelengths) UCF as obtained using the specified discrete-source approximation. The lower- and upper-bound peaks estimated from Eq. 5 are shown together with the actual pattern from Eq. 6. The pattern is cut-off at -40 dB to show the difference between the various plots more clearly.

Figure 4. One quadrant of the normalized, actual field of the 20-wavelength UCF compared with FM_{ave}. The circles indicate 34 of the 35 GM samples computed from Eq. 6 (one is below -60 dB), that were used in the estimation process. Because the cosine-angle values used to obtain the average and actual patterns do not always precisely match those used to obtain the original GM samples, some of the latter do not coincide with the pattern plots.
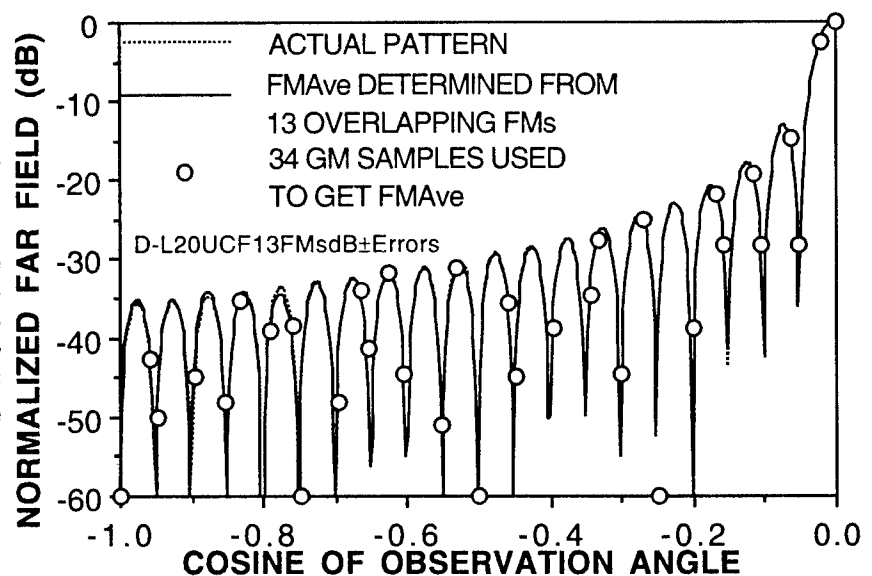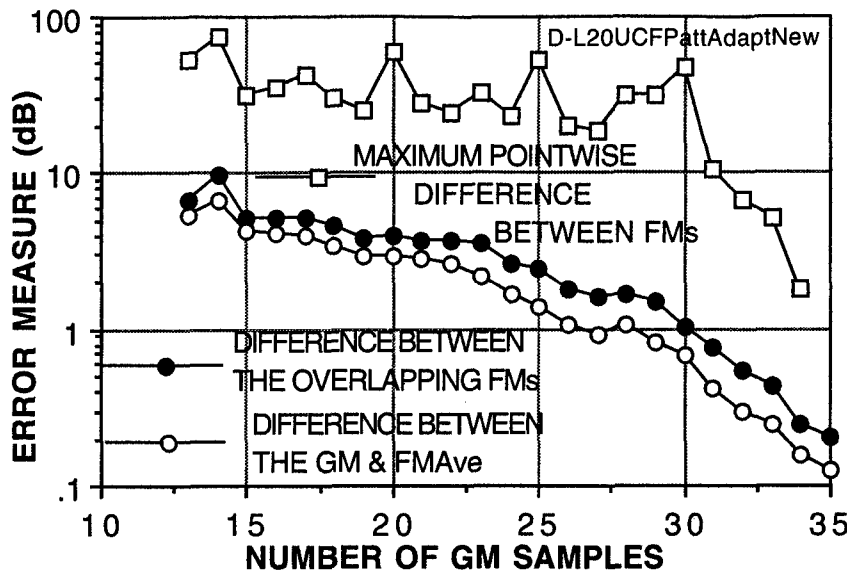
Figure 5. Three error measures discussed in the text for the UCF shown as a function of the number of GM samples used up to that point in the adaptation process over an observation window -90 to 0 deg, with the parameters in Eq. 3 given by $A_1 = 0.1$ dB and $A_2 = 0.05$ dB. The open squares denote the maximum pointwise difference between all pairs of overlapping FMs with the addition of a new GM sample. The closed and open circles exhibit the angle-averaged difference between the overlapping FMs and between the average FM and the GM itself. The fact that the latter is smaller than the former shows that the FM difference provides a conservative measure of the accuracy of FM_{ave}.

Figure 6. One quadrant of the normalized radiation pattern for the field of an L = 20 (wavelengths) SCF as obtained using the SDSA. The lower- and upper-bound peaks estimated from Eq. 5 are shown together with the actual field from Eq. 7. The pattern is plotted over a limited dB range to show the difference between the various plots more clearly.
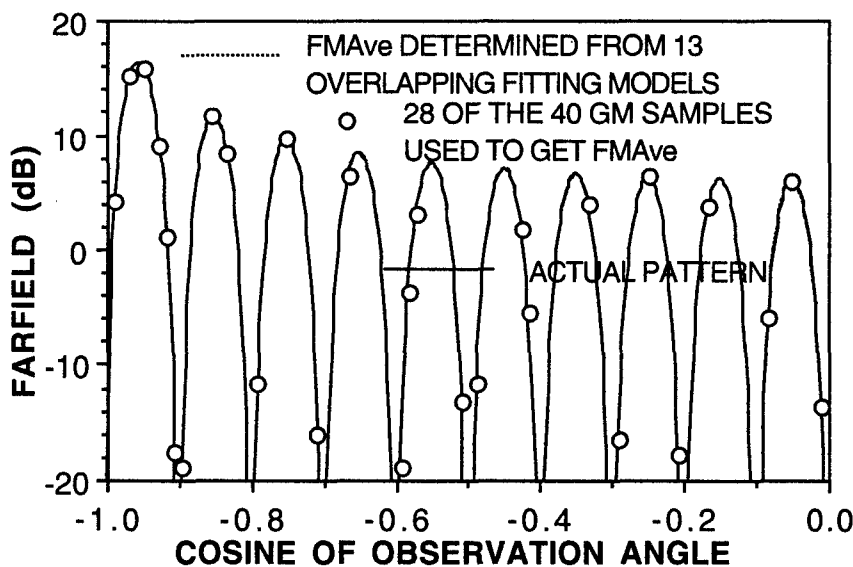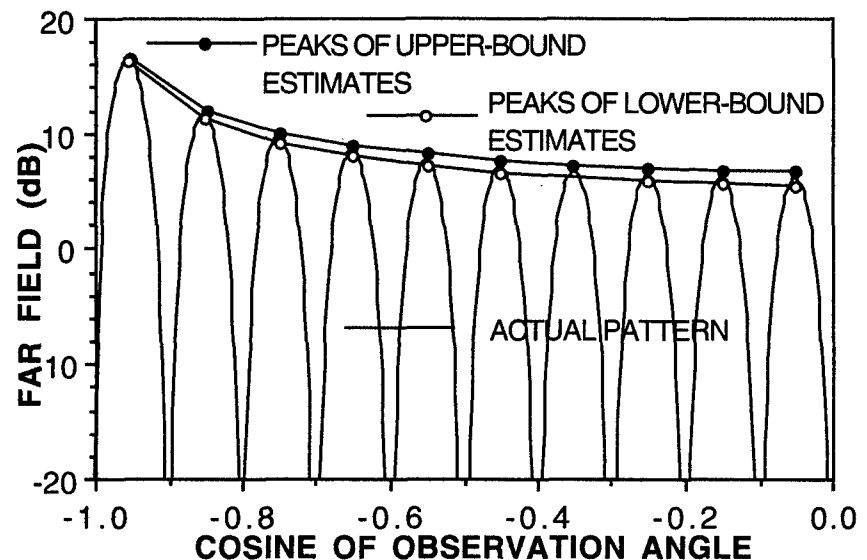

Figure 7. One quadrant of the actual field of the 20-wavelength SCF compared with FM_{ave}. The circles indicate 28 of the 40 GM samples, computed from Eq. 7, that were used in the estimation process.

4.2 The Far Radiated Field of the Sinusoidal Current Filament

The normalized far field of a center-fed sinusoidal current filament (SCF)°L wavelengths long is proportional to [10]

$$F_{SCF}(\theta) = \frac{\cos(\pi L \cos\theta) - \cos(\pi L)}{\sin\theta} \qquad (7)$$

Application of adaptive MBPE to an L = 20-wavelength SCF using N = 13 overlapping FMs as shown in Fig. 2 leads to the upper- and lower-bound estimates for the far field shown together with the actual pattern in Fig. 6. Again, the actual field values are seen to lie between the bounding curves provided by MBPE adaptive sampling. A comparison of FM_{ave} with the actual pattern is presented in Fig. 7 where most of the 40 GM samples used for the FM computation are also shown (some fall below - 20 dB). The actual and FM_{ave} curves are essentially graphically indistinguishable on the scale used. The 20-wavelength SCF has only 10 lobes rather than the 20 lobes of the 20-wavelength UCF over the same -1 to 0 cos(θ) interval, but requires 6 more unknowns to achieve the same estimation uncertainty, or 4 samples per lobe. This indicates that the number of GM samples needed to achieve a given pattern-estimation uncertainty is sensitive not only to the lobe structure of the pattern itself, but also to the spatial variation of the source distribution that produces that pattern.

4.3 The Far Field Scattered from a Thin, Circular Cylinder

The GM here is the approximate far, scattered field of a thin, circular cylinder L wavelengths long, which is proportional to [11]

$$RCS \propto F^2_{CYL}(\theta) = \left[\cos\theta_i \frac{\sin(2\pi L \sin\theta_i)}{2\pi L \sin\theta_i} \right]^2 \qquad (8)$$

for which MBPE adaptive sampling produces the results shown in Figs. 8 and 9 for L = 10 wavelengths with 7 FMs being used. In contrast with an L-wavelength SCF, where the number of lobes over a -1 to 0 interval in cos(θ) is ~ L/2 and the UCF which has ~ L lobes over that same interval, the L-wavelength scatterer has ~ 2L lobes, 20 in this example. As for the previous cases, the FM_{ave}, as obtained from 48 GM samples, and a finely sampled GM plot for the scatterer are graphically indistinguishable. The number of samples required per lobe for the 10-wavelength cylinder scatterer is thus 2.4, greater than the 1.75 needed for the UCF even though their patterns are quite similar, as can be seen by comparing Figs. 4 and 9.

4.4 The Far Radiated Field of a Randomized Array of Point Sources

The last example considered here is a linear array of 21, isotropic point sources having random amplitudes varying between -1 and +1 and located randomly within a 10-wavelength aperture. Results for cos(θ) varying from -1 to 0 are shown in Figs. 10 and 11, again using 13 FMs. A total of 26 GM samples is needed to achieve the same specified estimation error as used for the previous cases. Since there are on the order of 8.5 maxima in the pattern, this works out to about 3 samples per

lobe, midway between that required for the scatterer and the SCF. The number of samples needed per lobe or per wavelength of aperture to achieve the same specified estimation accuracy (as given by Eq. 3 with A_1 and A_2 0.1 dB and 0.05 dB, respectively) for the various sources considered here is summarized in Table I below.

5. CONCLUDING OBSERVATIONS CONCERNING ESTIMATION UNCERTAINTY AND SAMPLING

The preceding examples demonstrate that adaptive sampling of radiation and scattering patterns using MBPE with discrete-source-approximation FMs can be effective in not only reducing the number of samples needed to obtain a reduced-order, continuous representation of a pattern, but also in constraining the estimated pattern to satisfy an uncertainty specification. Some additional computations are included here to shed further light on the sampling requirements. The L = 20 UCF problem was repeated using A_1 = 0.05 and A_2 = 0 dB to reduce the estimation uncertainty to a smaller, and constant, value compared with the criterion used in obtaining the previous results. Using these coefficient values in the FME given by Eq. 3 results in a maximum acceptable difference between overlapping FMs, and hence, a maximum estimation error, of no more than 0.05 dB. This is much less than might normally be sought in practice but provides a more stringent test of the MBPE procedure. It should be noted that if the GM samples are of limited accuracy, for example being derived from a numerical first-principles model for a complex problem, then seeking an accuracy in the pattern estimate that the GM samples cannot provide might result in stagnating the estimation process, i.e., convergence may not occur. But when using an analytical expression for a pattern, as is done here, this will not be a problem. It s also worth noting that the variational relationship between the far fields and the sources that produce them results in errors in the latter not translating into comparable errors in the former.

Upon running the L = 20-wavelength UCF problem using these new values for the FME coefficients and plotting the same error measures as for Fig. 5, the results shown in Fig. 12 are obtained. Also included in Fig. 12 are lines of the form Aexp(-Bx) where x is the number of GM samples and A and B are best-fit parameters. It s interesting to see that the three best-fit lines are nearly parallel, with all decreasing exponentially as a function of the number of GM samples. This behavior is similar to the convergence of numerical solutions for various wire geometries as the number of unknowns in a moment-method solution is increased. A 0.1 dB in the angle-averaged FM difference and the difference between the FM_{ave} and the actual pattern is achieved using about 37 GM samples.

This computation was repeated for UCFs having lengths of L = 10, 15 and 25 wavelengths, yielding the results of in Fig. 13 where, for clarity, only the FM-FM differences are plotted. The data for each of these UCF°lengths are found to be fit comparably well by exponentials having different slopes. This is an expected result since the number of GM samples needed to achieve a given uncertainty for a specified source distribution is expected to be related to the number of pattern lobes which are, in turn, proportional to the aperture size. When the latter effect is removed by replotting the data of Fig. 13 as a function of the number of GM samples per wavelength of aperture, the results shown in Fig. 14 are obtained. The best-fit lines for the various

UCF lengths are nearly coincident, shifting to the left slightly with increasing L and exhibiting slopes that are within about 1.5%. A 0.1 dB angle-averaged FM difference is seen to require about 2 samples per wavelength of aperture.

Since a UCF L-wavelengths in extent produces L lobes per 90 deg in its pattern, this sampling density translates to about 2 samples per lobe as well. As can be deduced from Table I, it s clear that the far-field sampling density depends on more than just the lobe count in the pattern.
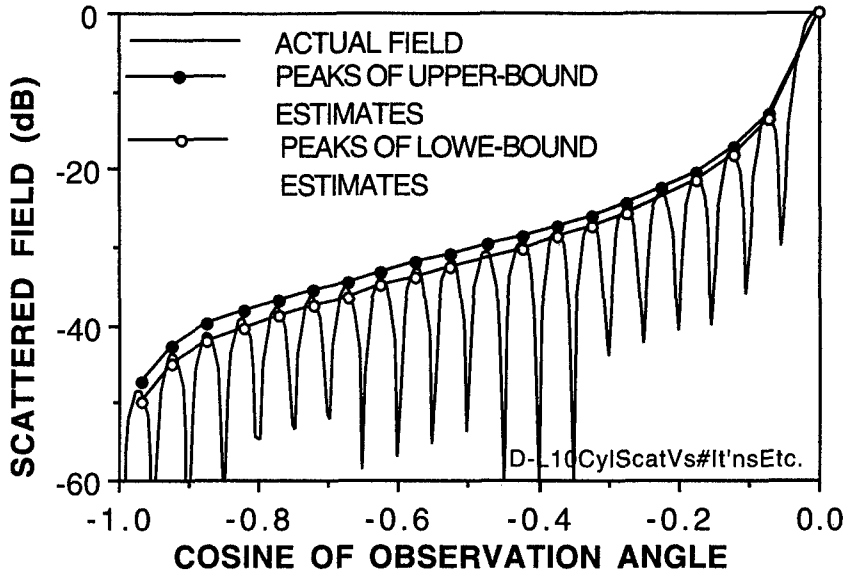
Figure 8. One quadrant of the normalized scattering pattern for the field of an L = 10 wavelengths thin cylinder as obtained using the SDSA. The lower- and upper -bound peak estimates of the far field from Eq. 5 are shown together with the actual field from Eq. 8.

Figure 9. One quadrant of the actual scattered field of the 10-wavelength cylinder compared with FM_{ave}. The circles indicate some of the 48 GM samples, computed from Eq. 8, that were used in the estimation process.
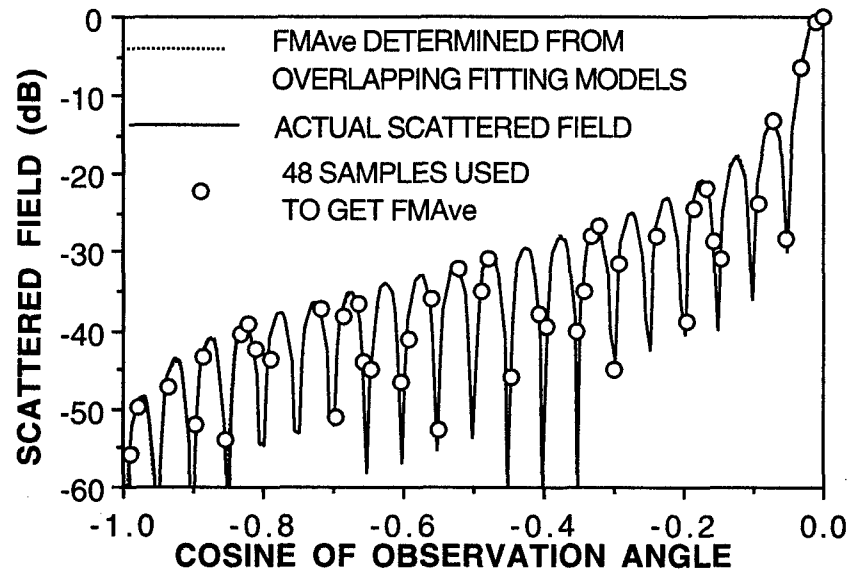
How this sampling density might generalize to 2D or 3D source distributions needs to be considered. First note that the sampling density of 2 per wavelength of aperture for the UCF applies to a pattern symmetric about broadside where an angle-observation window of only 90 deg needs to be sampled. For a non-symmetric, but otherwise equivalent, linear source distribution this would then work out to 4 samples per wavelength since a far-field window of 180 deg would then need to be sampled. For a true 2D source whose pattern has to be sampled over 360 deg, this would imply that 8 samples per wavelength of its maximum linear aperture are needed to achieve a comparable pattern accuracy of 0.1 dB. This measure would seem to hold in planar

cuts for the radiation patterns of 3D source distributions as well.

Results obtained for the cylinder scatterer indicate, on the other hand, that nearly 5 samples per wavelength of cylinder length are required for the same kind of pattern-estimation accuracy for a 90-deg sector of the scattered field to be estimated. Following the same line of reasoning as above for a general 2D scatterer, or for planar cuts of 3D objects, sampling over 360 deg can be estimated to require on the order of 20 samples per wavelength. One obvious question arises about why a greater sampling density is apparently needed for a scattering pattern as compared with a radiation pattern when the two are similar-appearing, as exhib-

ited by Figs. 4 and 9? Perhaps the answer is that for the latter situation a single current distribution produces the entire radiated field. For the former, on the other hand, the current distribution, being a function of the angle of incidence, changes with every viewing angle when determining the monostatic radar cross section.

It would also seem to follow then that the number of GM samples needed to achieve a specified estimation uncertainty must depend on both the aperture size and spatial variation of the source within it, a dependence that ultimately is exhibited by the pattern rank (R) or the number of degrees of freedom of the pattern, over the chosen observation window. As a specific example of how the source characteristics and aperture might influence the rank, consider an aperture L-wavelengths long having N point sources uniformly spaced within it.

For the simplest case of two point sources, as L is increased, the number of pattern lobes over 360 deg in an observation plane containing the sources will be of order 4L. However, R, as determined by eigenvalue analysis of the data matrix that arises when using Prony s method remains fixed at two when L exceeds 0.5, regardless of how large the aperture is made and how many lobes are in the pattern. On the other hand, if L is fixed and the number of point sources is systematically increased, R will increase proportionately until N > 2L whereupon R remains fixed at ~ 2L since only about 2 source/wavelength can be resolved in the far field. Because it can model such point-source arrays, a Prony-based procedure can exploit the reduced rank of such special problems, but the discrete-source approximation and a Fourier model of the far field are not as well-suited for doing so. Generally speaking, with everything else being equal, the best pattern estimator would be one for which the number of GM samples can be reduced to as close to R as possible. More investigation is needed to settle these issues, and to generalize the results beyond the simple cases considered here.
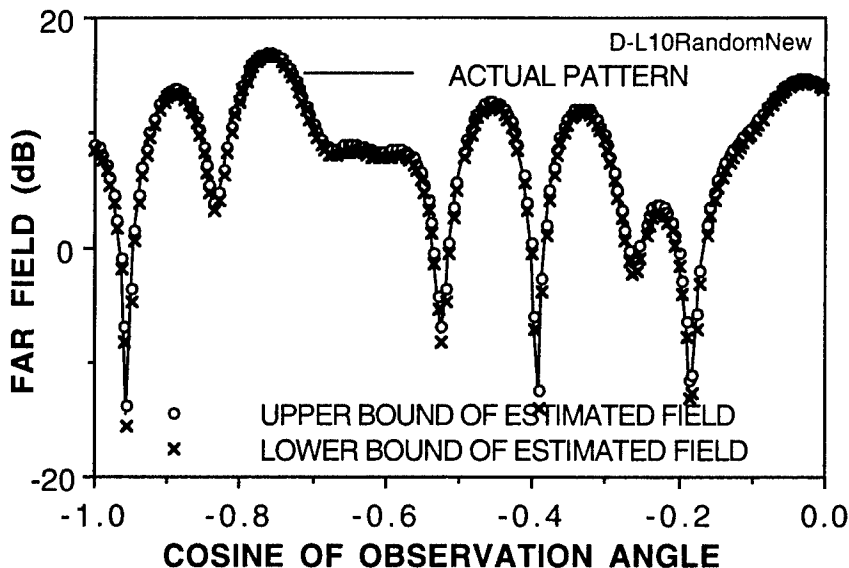

Figure 10. One quadrant of the radiation pattern for the field of 21 isotropic point sources having random amplitudes between -1 and + 1 and randomly located along a an L = 10 wavelengths linear array. Upper-bound estimates of the pattern are shown by the x's and the lower-bound estimates by the open circles with the actual pattern shown by the solid line.

Figure 11. The actual pattern of 21 isotropic sources having random amplitudes and located at random positions along a 10-wavelength aperture compared with FM_{ave}. The circles indicate the 26 GM samples used in the estimation process.
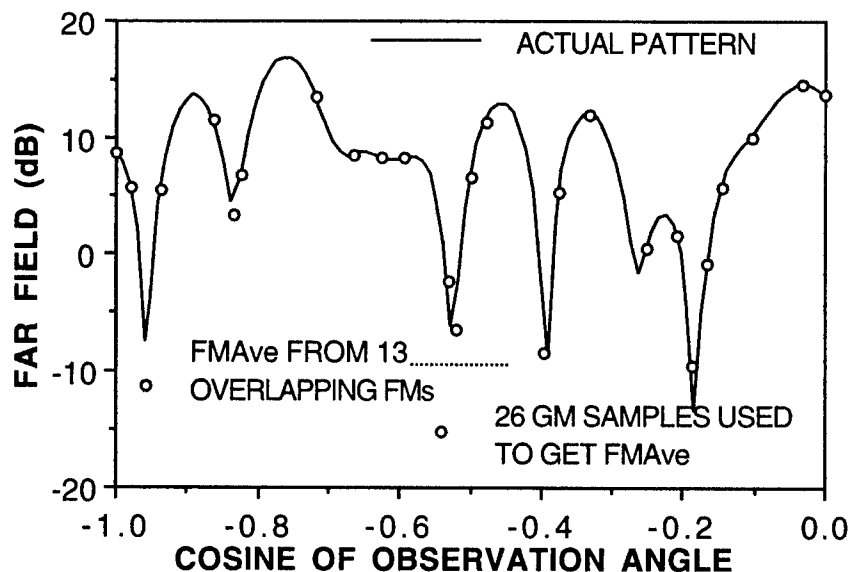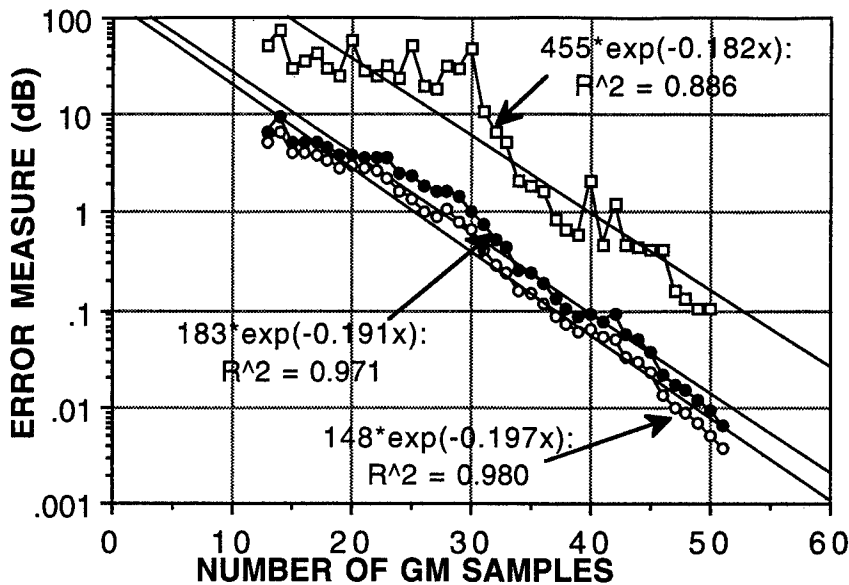
Figure 12. The three error measures shown in Figure 6 are plotted here for the 20-wavelength UCF but with $A_1 = 0.05$ and $A_2 = 0$ in Eq. 3 to obtain an estimate that is both more accurate and remains constant over the dynamic range covered by the pattern sampled in a -90 to 0 deg observation window. A best-fit straight line is computed for all three, where R^2 is the square of the correlation coefficient. All three best-fit lines are seen to be nearly parallel on this log-linear plot, being well-described as exponential functions of the number of GM samples.
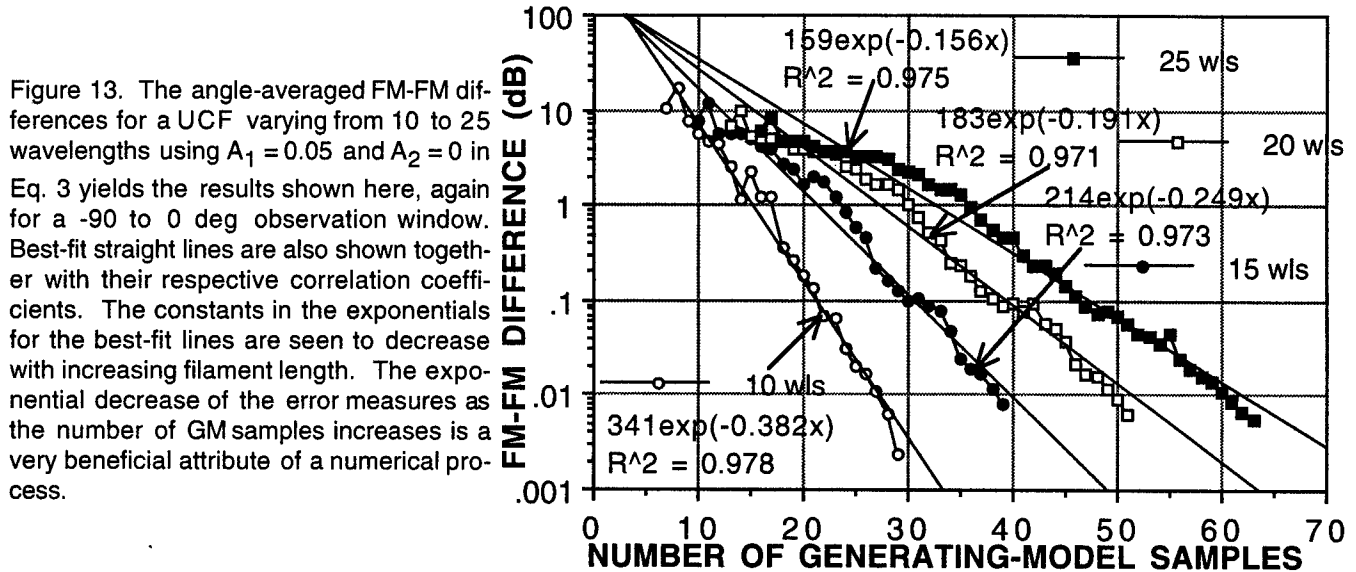
Figure 13. The angle-averaged FM-FM differences for a UCF varying from 10 to 25 wavelengths using $A_1 = 0.05$ and $A_2 = 0$ in Eq. 3 yields the results shown here, again for a -90 to 0 deg observation window. Best-fit straight lines are also shown together with their respective correlation coefficients. The constants in the exponentials for the best-fit lines are seen to decrease with increasing filament length. The exponential decrease of the error measures as the number of GM samples increases is a very beneficial attribute of a numerical process.
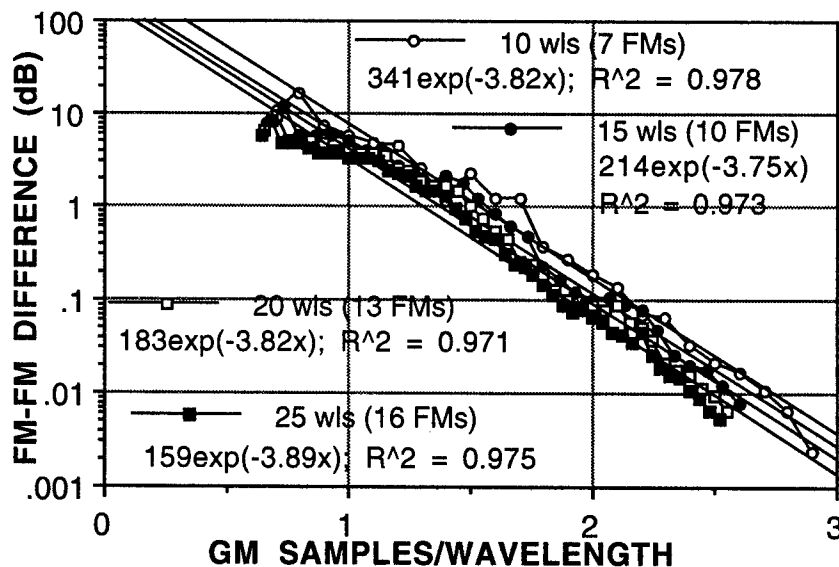

Figure 14. Upon replotting the results of Fig. 13 but with the number of GM samples/wavelength as the independent variable, the best-fit angle-averaged FM-FM differences become nearly coincident. These results show that for this particular case the number of GM samples needed for a specified angle-averaged FM difference in the pattern is linearly proportional to the filament length. They also show that the sampling density required for a given value of error measure decreases somewhat as the UCF increases in length.

TABLE I: FAR-FIELD SAMPLING REQUIRED OVER A 90-
deg WINDOW FOR SOURCES TESTED USING $A_1 = 0.1$
AND $A_2 = 0.05$ dB in Eq. 3.

SOURCE TYPE TESTED	NUMBER OF SAMPLES	FAR-FIELD SAMPLES/ LOBE	FAR-FIELD SAMPLES/ WAVELENGTH OF APERTURE
20-WL SINUSOIDAL CURRENT FILAMENT	40	4	2
10-WL RANDOMIZED ARRAY	26	3	2.6
10-WL CYLINDER SCATTERER	48	2.4	4.8
20-WL UNIFORM CURRENT FILAMENT	35	1.75	1.75

5. REFERENCES

1. E. K. Miller (1995), Model-Based Parameter Estimation in Electromagnetics: I--Background and Theoretical Development, *Applied Computational Electromagnetics Society Newsletter*, 10 (3), November, pp. 40-63; (1996), II--Applications to EM Observables, 11 (1), pp. 35-56; (1995), III--Applications to EM Integral Equations, *Applied Comptational Electromagnetics Society Journal*, 10 (3), pp. 9-29.

2. E. K. Miller (1998), Computing Radiation and Scattering Patterns Using Model-Based Parameter Estimation, *IEEE AP-S International Symposium*, Renaissance Waverly Hotel, Atlanta, GA, June 21-26, pp. 66-69.

3. E. K. Miller and T. K. Sarkar (1999), An Introduction to the Use of Model-Based Parameter Estimation in Electromagnetics, in *Review of Radio Science*, 1999 URSI General Assembly, pp. 139-174.

4. R. J. Allard, D. H. Werner, J. S. Zmyslo, and P. L. Werner, "Spectral Domain Interpolation of Antenna Radiation Patterns Using Model-Based Parameter Estimation and Genetic Algorithms", *Proceedings of the 14th Annual Review of Progress in Applied Computational Electromagnetics (ACES)*, Vol. 2, pp. 964-971, 1998.

5. D. H. Werner and R. J. Allard, "The Simultaneous Interpolation of Antenna Radiation Patterns in Both the Spatial and Frequency Domains Using Model-Based Parameter Estimation", *IEEE Transactions on Antennas and Propagation*, Vol. 48, No. 3, pp. 383-392, 2000.

6. O. M. Bucci and G. Franceschetti, On the Degrees of Freedom of Scattered Fields, *IEEE Antennas and Propagation Society Transactions*, Vol. 37, No. 7, pp. 918-929, July 1989.

7. O. M. Bucci, C. Gennarelli and C. Savarese, Optimal Interpolation of Radiated Fields Over a Sphere, *IEEE Antennas and Propagation Society Transactions*, Vol. 39, No. 11, pp. 1633-1643, November 1991.

8. O. M. Bucci, C. Gennarelli and C. Savarese, Representation of Electromagnetic fields Over Arbitrary Surfaces by a Finite and Nonredundant Number of Samples, *IEEE Antennas and Propagation Society Transactions*, Vol. 46, No. 3, pp. 315-359, March 1998.

9. R. W. Hamming, *Numerical Methods for Scientists and Engineers*, Dover Publications, Inc., New York, 1962.

10. C. A. Balanis, *Antenna Theory: Analysis and Design*, Harper & Row, Publishers, New York, 1982.

11. E. G. Knott, J. F. Shaeffer and M. T. Tuley, *Radar Cross Section*, 2nd Edition, Artech House, Boston, 1993.

ACRONYMS

DSA--Discrete-Source Approximation
FM--Fitting Model
FME--Fitting-Model Error
FSPM--Fourier Series Pattern Model
GM--Generating Model
MBPE--Model-Based Parameter Estimation
OC--Operation Count
PDSA--Prony Discrete-Source Approximation
R--Rank
RCS--Radar Cross Section
SCF--Sinusoidal Current Filament
SDSA--Specified Discrete-Source Approximation
UCF--Uniform Current Filament
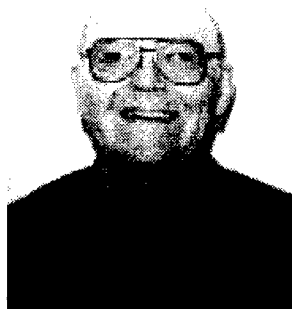
Edmund K. Miller earned a B.S.E.E. at Michigan Technological University and an M.S.Nuc.E., an M.S.E.E. and a Ph.D.E.E. at the University of Michigan. His work experience includes the Radiation and High Altitude Engineering Laboratories of the U. of Michigan, Lawrence Livermore and Los Alamos National Laboratories, and MBAssociates, Rockwell International Science Center and General Research Corporation. He has been a physics instructor at Michigan Technological University, a Regents-Distinguished Professor at the University of Kansas and a Stocker Visiting Professor at Ohio University. He has also been a Guest Scientist at the University of Pretoria and University of Stellenbosch, both in the Republic of South Africa. Dr. Miller is presently actively retired in Santa Fe, NM.

He has served two terms on IEEE AP-S AdCom and has been an AP-S Distinguished Lecturer. He was elected IEEE Fellow in 1994 and received the IEEE Third Millennium Medal in 2000. He was the recipient (with co-authors) of the 1988 Best Paper Award from the IEEE Education Society. He has served on the Editorial Board of IEEE student magazine *POTENTIALS* since 1985 and was its Editor 1992-1995. Dr. Miller served as the first President of ACES and two terms on the ACES Board of Directors. His primary interests remain focused on computational electromagnetics, applied signal processing, visual electromagnetics, and promoting the incorporation of accuracy statements in CEM numerical results.